Molecular Human Reproduction, Vol.25, No.5 pp. 241–256, 2019
Advanced Access publication on March 13, 2019 doi:10.1093/molehr/gaz015

molecular human reproduction

ORIGINAL ARTICLE

Differential cell death decisions in the testis: evidence for an exclusive window of ferroptosis in round spermatids

Elizabeth G. Bromfield [1,*], Jessica L.H. Walters[1], Shenae L. Cafe[1], Ilana R. Bernstein[1], Simone J. Stanger[1], Amanda L. Anderson[1], R. John Aitken [1], Eileen A. McLaughlin[2], Matthew D. Dun[3], Barend M. Gadella[4,5], and Brett Nixon [1]

[1]Priority Research Centre for Reproductive Science, School of Environmental and Life Sciences, Discipline of Biological Sciences, University of Newcastle, University Drive, Callaghan, New South Wales, 2308, Australia [2]School of Biological Science, University of Auckland, Auckland, 1010, New Zealand [3]Priority Research Centre for Cancer Research, Innovation and Translation, Hunter Medical Research Institute, School of Biomedical Sciences and Pharmacy, Faculty of Health and Medicine, University of Newcastle, University Drive, Callaghan, New South Wales, 2308, Australia [4]Department of Biochemistry and Cell Biology, Faculty of Veterinary Medicine, Utrecht University, Yalelaan 2, 3584 CM, Utrecht, The Netherlands [5]Department of Farm Animal Health, Faculty of Veterinary Medicine, Utrecht University, Yalelaan 2, 3584 CM, Utrecht, The Netherlands

*Correspondence address. The University of Newcastle, University Drive, Callaghan, New South Wales 2308, Australia. Tel: +61-24-92-1627; E-mail: elizabeth.bromfield@newcastle.edu.au orcid.org/0000-0001-7256-1403

Submitted on November 11, 2018; resubmitted on January 25, 2019; editorial decision on February 27, 2019; accepted on March 4, 2019

Oxidative stress is a major aetiology in many pathologies, including that of male infertility. Recent evidence in somatic cells has linked oxidative stress to the induction of a novel cell death modality termed ferroptosis. However, the induction of this iron-regulated, caspase-independent cell death pathway has never been explored outside of the soma. Ferroptosis is initiated through the inactivation of the lipid repair enzyme glutathione peroxidase 4 (GPX4) and is exacerbated by the activity of arachidonate 15-lipoxygenase (ALOX15), a lipoxygenase enzyme that facilitates lipid degradation. Here, we demonstrate that male germ cells of the mouse exhibit hallmarks of ferroptosis including; a caspase-independent decline in viability following exposure to oxidative stress conditions induced by the electrophile 4-hydroxynonenal or the ferroptosis activators (erastin and RSL3), as well as a reciprocal upregulation of ALOX15 and down regulation of GPX4 protein expression. Moreover, the round spermatid developmental stage may be sensitized to ferroptosis via the action of acyl-CoA synthetase long-chain family member 4 (ACSL4), which modifies membrane lipid composition in a manner favourable to lipid peroxidation. This work provides a clear impetus to explore the contribution of ferroptosis to the demise of germline cells during periods of acute stress in *in vivo* models.

Key words: ferroptosis / oxidative stress / germ cell / lipid peroxidation / lipoxygenase / infertility / cell death / spermatid

Introduction

The peroxidation of biomembranes and subsequent accumulation of lipid hydroperoxides within cells is known to promote cellular demise across a wide range of cell types (Ayala *et al.*, 2014; Gaschler and Stockwell, 2017; Maiorino *et al.*, 2018). As such, the study of enzymes that contribute to lipid peroxidation or regulate its deleterious outcomes has been gaining traction (Yamamoto, 1991; Noguchi *et al.*, 2002; Shintoku *et al.*, 2017). One class of enzymes; the lipoxygenases, which catalyze the oxygenation and degradation of polyunsaturated fatty acids (PUFAs), have been given particular consideration due to their widespread role in the onset of diseases. Examples include ischaemic heart disease, Alzheimer's disease, chronic myeloid leukaemia, diabetes and colorectal cancer, all of which are linked to an elevation of the lipid peroxidation product 4-hydroxynonenal (4HNE) (Martínez-Clemente *et al.*, 2010; Chen *et al.*, 2014; Chu *et al.*, 2015; Mao *et al.*, 2015; Suzuki *et al.*, 2015; Lundqvist *et al.*, 2016; Yang *et al.*, 2016). 4HNE, the most widely studied and cytotoxic of the lipid aldehydes, is known to be produced through enzymatic transformation of *n*–6 PUFAs (arachidonic acid (AA), linoleic acid and others) by 15-lipoxygenases (Ayala *et al.*, 2014). This capacity for 4HNE to induce cell death is largely reliant on its ability to covalently modify DNA as

well as selective elements of the cell proteome (Hu et al., 2002; Ivanov et al., 2010; Aitken et al., 2012; Zhong and Yin, 2014).

While this cytotoxic cascade is a well-recognized paradigm in somatic cells, we have recently established that 4HNE modification also contributes to severe changes in protein homeostasis within the male germline, including a precipitous loss of key proteins required for sperm–egg recognition (Bromfield et al., 2015, 2017a). In a comprehensive analysis of arachidonate 15-lipoxygenase (ALOX15) in the male germline we have now reported a robust upregulation of ALOX15 in response to oxidative stress in primary cultures of round spermatids from the mouse testis and subsequently demonstrated a protective effect on cell viability, and decreased lipid peroxidation through the pharmacological inhibition of ALOX15 (Bromfield et al., 2017b). Moreover, the inhibition of ALOX15 in mature human spermatozoa results in a significant reduction in 4HNE and a complete recovery of human sperm–egg interaction, a requisite step to fertilization that is compromised by oxidative stress (Walters et al., 2018). Combined, our data establish ALOX15 as an important physiological target to prevent oxidative stress-induced pathologies in developing germ cells of the mouse testis and in mature human spermatozoa. However, a key observation of these studies lies in the remarkable specificity of this response to the round spermatid stage of germ cell development. Thus, modulation of ALOX15 overexpression in response to oxidative challenge is only detected in round spermatids and not in the earlier developmental stage pachytene spermatocytes isolated from the same animals (Bromfield et al., 2017b). Accordingly, the round spermatid stage appears to be a critical point in germ cell maturation where these cells become extremely susceptible to lipid peroxidation, 4HNE production and an associated instability of 4HNE-modified protein targets such as heat shock protein A2 (HSPA2) (Bromfield et al., 2017a). Combined, these observations in the round spermatid population accord with recent findings in somatic cells that implicate ALOX15 in the induction of a novel form of cell death termed 'ferroptosis'.

Ferroptosis is an iron-regulated, caspase-independent cell death modality that was first reported in 2012 (Dixon et al., 2012) and has since been implicated in lipid-peroxidation induced cell death across an array of disease states, tissues and cell types (Skouta et al., 2014; Yang et al., 2014; Ingold et al., 2015; Matsushita et al., 2015). Ferroptosis is initiated through a loss of activity of the lipid repair enzyme, glutathione peroxidase 4 (GPX4), and/or an inhibition of cysteine uptake, causing a depletion of glutathione (GSH) and concluding in a lethal accumulation of reactive oxygen metabolites (Dixon et al., 2012; Yang et al., 2014; Doll and Conrad, 2017). A pivotal role for lipoxygenases in this process has been reported in acute lymphoblastic leukaemia cells (Probst et al., 2017), airway epithelial cells in asthma and cortical and hippocampal neurons in brain trauma (Wenzel et al., 2017). A conserved signature of lipoxygenase action in these pathologies is the catalytic production of abundant lipid hydroperoxides, which in turn serve as the key death signals in the ferroptotic cascade (Shintoku et al., 2017; Wenzel et al., 2017). Compellingly, ferroptotic cell death induced by either erastin, a ferroptosis activator that inhibits the cystine-glutamate antiporter System Xc^-, or RSL3, a direct inhibitor of GPX4, can be tempered by siRNA knockdown of ALOX15 or pharmacological inhibition of the protein, suggesting that ALOX15 expression sensitizes cells to ferroptosis (Yang et al., 2016; Shintoku et al., 2017).

In the testis, a similar paradoxical relationship between ALOX15 and GPX4 exists whereby germline inactivation of the *Alox15* gene rescues the male subfertility induced by heterozygous expression of catalytically silent GPX4 (Brütsch et al., 2016). Despite this knowledge, the contribution of ALOX15 enzymatic activity to the onset of ferroptotic cell death in the germline has never been explored. Given our observations of the differential sensitivity of pachytene spermatocytes and round spermatids to oxidative stress, this study was designed to evaluate key correlates of ferroptosis in the male germline in response to oxidative stress, explore the involvement of ALOX15 in this process and examine developmental differences in cell death decisions in the testis.

Materials and Methods

Ethics approval

All experimental procedures involving mice were conducted with the approval of the University of Newcastle (UoN) Animal Care and Ethics Committee (ACEC) (Approval numbers A-2013-322 and A-2018-826). Swiss mice were obtained from a breeding colony held at the UoN central animal facility and maintained according to the recommendations prescribed by the ACEC. Mice were housed under a controlled lighting regime (16L:8D) at 21–22°C and supplied with food and water *ad libitum*. The human semen samples used in this study were obtained with informed consent from a panel of normozoospermic donors as part of the UoN human sperm donation programme facilitated by the Priority Research Centre for Reproductive Science. All studies were performed in accordance with the University of Newcastle's Human Ethics Committee guidelines (Approval No. H-2013-0319).

Antibodies and reagents

Unless otherwise specified, all reagents were purchased from Sigma-Aldrich (St Louis, MO, USA) and were of research grade. All antibodies were purchased from Abcam (Cambridge, UK) unless otherwise stated and used as shown in Supplementary Table SI.

Mouse spermatocyte and spermatid preparation

Enriched populations of pachytene spermatocytes and round spermatids were acquired from dissected adult (>8 weeks old) Swiss mouse testes using density sedimentation at unit gravity, as described previously (Baleato et al., 2005; Nixon et al., 2014; Bromfield et al., 2017b). Testes were disassociated and tubules were sequentially digested with 0.5 mg/ml collagenase/DMEM and 0.5% v/v trypsin/ EDTA to remove extratubular contents and interstitial cells. The remaining isolated cells were loaded onto a 2–4% w/v bovine serum albumin (BSA)/DMEM gradient to separate male germ cell types according to density. This method resulted in the isolation of pachytene spermatocytes (~93% purity) and round spermatids (~86% purity) with very little to no somatic cell contamination, as verified by staining preparations with the nuclear stain (4′,6-diamidino-2-phenylindole) DAPI, and additionally through dual labelling of phosphorylated histone H2AX with anti-γH2AX (to label pachytene spermatocytes) and peanut lectin agglutintin (to label the developing acrosome of round spermatids). Cell preparations were viewed with a Zeiss Axioplan 2 fluorescence microscope (Carl Zeiss MicroImaging GmbH, Jena, Germany) and the percentage of round spermatids and pachytene spermatocytes with the appropriate labelling was recorded for each population (Supplementary Fig. S1A). Unless otherwise specified, spermatocytes and spermatids were pooled from 2 to 4 mice to achieve adequate cell numbers for analysis. Experiments on pooled samples were

conducted on three independent replicates for subsequent statistical analysis by ANOVA.

Preparation of mouse and human spermatozoa

Mouse spermatozoa were isolated from the cauda epididymidis of adult Swiss mice into pre-warmed microcapillary tubes by a method of retrograde perfusion (Smith *et al.*, 2013) and further released into Biggers, Whitten and Whittingham medium (BWW). Human semen samples were collected following sexual abstinence of at least 2 days. After collection, all samples were kept at 37°C with sample analysis initiated after completion of liquefaction and within 1 h of ejaculation. Human semen samples were fractionated over a discontinuous Percoll density gradient (comprising 40 and 80% Percoll suspensions) by centrifugation at 500 *g* for 30 min (Redgrove *et al.*, 2012). The sperm cells collected from the base of the 80% Percoll suspension are nominally referred to as 'good quality' or 'mature' spermatozoa, whereas those partitioning at the 40/80% Percoll interface are referred to as 'poor quality' spermatozoa (Aitken *et al.*, 1993). Unless otherwise stated, good quality spermatozoa were used throughout our experiments. After centrifugation, the pellets at the base of the 80% Percoll suspensions were collected individually prior to being resuspended in BWW. These cells were washed by centrifugation at 500 *g* for 15 min and again resuspended in BWW prior to use in the specified experiments. A routine assessment of semen parameters was conducted for all donors in accordance with World Health Organization (WHO) criteria and corresponding to the checklist published by Björndahl *et al.* (2016). At least 100 cells were assessed for determination of cell motility, viability and morphology, with at least five microscope fields of view being examined in each count. Sperm morphology was assessed in accordance with WHO criteria using ×400 magnification and bright field microscopy (Olympus CX40, Olympus, Sydney, Australia). Motility assessment was performed using phase contrast microscope optics (×400 magnification), with cells being classified as either motile (i.e. sperm that displayed any form of motility ranging from rapid progressive to non-progressive) or immotile.

Induction of oxidative stress

In accordance with our previously established protocols, lipid peroxidation and oxidative stress were induced in germ cells and mature spermatozoa using 4HNE obtained from Cayman chemicals (Ann Arbor, MI, USA). To demonstrate a dose-dependent decline in cell viability in pachytene spermatocytes and round spermatids and investigate the nature of this cell death, concentrations of 100–400 μM 4HNE were initially used; such doses being within the range of 4HNE concentrations normally associated with oxidative stress *in vivo* (Uchida *et al.*, 2003; Chen and Niki, 2006). Thereafter, 100 μM 4HNE was used in all assays to induce oxidative stress in precursor germ cells. For mature human and mouse spermatozoa, 100 μM 4HNE was used. For all cells, the induction of low levels of oxidative stress involved incubation in 4HNE for 1 h at 37°C, followed by centrifugation at 500 *g* for 3 min and resuspension in pre-warmed DMEM (for germ cells) or pre-warmed BWW (for spermatozoa) to remove residual 4HNE. Importantly, the use of these conditions consistently promoted an average range of 30–40% cell death in round spermatid populations and 15–25% cell death in pachytene spermatocytes.

Induction of ferroptosis with erastin and RSL3

To determine whether ferroptosis could be induced chemically in the male germline, germ cells were incubated in 10, 20 and 40 μM erastin and 0.1, 1 and 10 μM RSL3 and held at 37°C for 1 h. These concentrations were selected based on their use in previous publications characterizing ferroptosis in cell lines and adjusted for use in the short incubation times documented in this study (Dixon *et al.*, 2014; Dächert *et al.*, 2016; Shintoku *et al.*, 2017). Following an analysis of the resulting cell death percentages in pachytene spermatocytes and round spermatids, concentrations of 20 μM erastin and 1 μM RSL3 were used throughout these studies.

Cell viability and assessment of apoptotic cell death

Cell viability was assessed using two independent methods, namely the incorporation of Eosin Y into non-viable cells and assessment of this staining via light microscopy (pink = dead, no stain = viable), or incorporation of propidium iodide (PI) into non-viable cells, and assessment using fluorescence microscopy (red cells = dead, no fluorescence = viable). Both techniques obtained statistically similar results. The specific use of either Eosin Y or PI in each experiment is stated in all relevant figure captions in this article. To determine whether cells exposed to 4HNE had initiated apoptosis-/caspase-dependent cell death, two independent fluorescence-based assays were used on round spermatids and pachytene spermatocytes. Caspase activation was observed using fluorochrome-labelled inhibitor of caspase activity (FLICA) reagents purchased from Thermo Fisher Scientific (North Ryde, NSW, Australia). Similarly, phosphatidylserine externalization was observed with Annexin V-FITC also purchased from Thermo Fisher Scientific. The use of these two assays permitted the assessment of two key events of early-mid apoptosis. Assays were performed in accordance with our previously published protocols (Koppers *et al.*, 2011) and the manufacturer's instructions.

Immunodetection of ALOX15, GPX4 and ACSL4

Following the induction of oxidative stress or ferroptosis, round spermatids and pachytene spermatocytes were fixed in 4% paraformaldehyde for 15 min at room temperature, washed 3× with 0.05 M glycine in phosphate-buffered saline (PBS) and then pipetted onto poly-L-lysine-coated glass coverslips and allowed to settle overnight at 4°C. Subsequently, cells were permeabilized with 0.2% Triton X-100 for 15 min, then placed in a humid chamber and blocked in 3% BSA/PBS for 1 h at 37°C. Coverslips were washed in PBS (3 × 5 min) and incubated in anti-ALOX15, anti-acyl-CoA synthetase long-chain family member 4 (ACSL4), or anti-GPX4 antibodies diluted 1:100 (concentrations found in Supplementary Table SI), overnight at 4°C. Following this, coverslips were washed (3 × 5 min) in PBS at room temperature before applying appropriate secondary antibodies diluted 1:100 with 1% BSA/PBS for 1 h at room temperature. Coverslips were washed in PBS (3 × 5 min) before mounting in 10% Mowiol 4–88 (Merck, Frenchs Forest, NSW, Australia) with 30% glycerol in 0.2 M Tris (pH 8.5) and 2.5% 1,4-diazabicyclo-(2.2.2)-octane. Cell labelling was examined with a Zeiss LSM510 laser scanning confocal microscope (Carl Zeiss Pty, Sydney, Australia). Fluorescence intensity analysis was performed by recording the fluorescence of at least 50 isolated germ cells over three replicates using Image J software (National Institutes of Health, USA; version 1.51j8) where the area and integrated density of each cell was measured. The average of the mean background was determined for secondary antibody only probed germ cells. Fluorescence intensity for each population was then determined by subtracting the area × the mean background from the integrated density. Peripheral membrane localization of ACSL4 and ALOX15 was determined through visualization of pachytene spermatocytes and round spermatids. Those with a complete ring of fluorescence at the plasma membrane were recorded as positive for peripheral labelling. This assay provides an indication of membrane versus cytosolic immunofluorescence. Imaging was performed using an Olympus FV1000 confocal

using a 60×/1.2 NA UPLSAPO oil immersion objective lens (Olympus, Australia). Cells were scored as 'positive' for membrane labelling when clear peripheral labelling was observed. At least 50 cells per replicate were scored for four biological replicates. Images of each labelling pattern are included for visual clarity.

SDS-polyacrylamide gel electrophoresis and immunoblotting

Protein was extracted from all cells via boiling in sodium dodecylsulphate (SDS) extraction buffer (0.375 M Tris pH 6.8, 2% w/v SDS, 10% w/v sucrose, protease inhibitor cocktail) at 100°C for 5 min. Insoluble material was removed by centrifugation (17 000 *g*, 10 min, 4°C) and soluble protein remaining in the supernatant was quantified using a DC protein assay kit (Bio-Rad, Gladesville, NSW, Australia). Equivalent amounts of protein (either 2.5 or 5 µg, as specified in each figure legend) were boiled in SDS-polyacrylamide gel electrophoresis (PAGE) sample buffer (2% v/v mercaptoethanol, 2% w/v SDS, and 10% w/v sucrose in 0.375 M Tris, pH 6.8, with bromophenol blue) at 100°C for 5 min, prior to being resolved by SDS-PAGE (150 V, 1 h) and transferred to nitrocellulose membranes (350 mA, 1 h). Membranes were then blocked and incubated with appropriate antibodies raised against target proteins by using optimized conditions as previous described (Bromfield *et al.*, 2017a). Briefly, blots were washed 3 × 10 min at room temperature with Tris-buffered saline (TBS) supplemented with 0.1% (v/v) Tween-20 (TBST), before being probed with appropriate horse-radish peroxidase-conjugated secondary antibodies (Supplementary Table SI). After three further washes, labelled proteins were detected using an enhanced chemiluminescence kit (GE Healthcare, Silverwater, New South Wales, Australia). Where appropriate, protein band intensity relative to an anti-α-tubulin loading control was determined by densitometry using Image J software (Gassmann *et al.*, 2009).

Manipulation of ferroptosis: ferrostatin-1 and deferoxamine

Ferrostatin-1 (FER-1), a well-characterized ferroptosis inhibitor (Zilka *et al.*, 2017) was used to confirm the induction of ferroptosis in round spermatids under conditions of oxidative stress. The 2 µM concentration of FER-1 used in these assays was based on previously published findings (Dixon *et al.*, 2012). Round spermatids and pachytene spermatocytes were pre-treated with FER-1 for 30 min at 37°C, prior to the addition of 100 µM 4HNE for 1 h at 37°C. Additionally, to assess the dependency of this cell death phenomenon on the presence of iron, the iron chelator deferoxamine (DEF) was used in a similar pre-treatment strategy. For this assay, pachytene spermatocytes and round spermatids were treated with 100 µM DEF for 1 h at 37°C prior to the addition of 4HNE as above. Importantly, FER-1 and DEF only controls were used to dissect the effect of 4HNE on cell death under conditions refractory to ferroptosis. In both experiments, all cells were washed in pre-warmed DMEM after 4HNE incubations and assessed for cell death using PI and FLICA, as described above.

Inhibition of ALOX15 and ACSL4

Inhibition of ALOX15 activity in round spermatids was performed using the indole-based inhibitor 6,11-dihydro[1]benzothiopyrano[4,3-b]indole (PD146176; Tocris Bioscience, Avonmouth, Bristol, UK). PD146176 is a non-competitive, ALOX15 specific inhibitor (Sendobry *et al.*, 1997; Sadeghian and Jabbari, 2015) that is known to significantly reduce 15-HPETE and HODE, major products of the ALOX15 metabolic pathway. The concentration of PD146176 used in this study, 0.5 µM, was selected based on the IC_{50} of PD146176 in rabbit reticulocytes (0.54 µM) and validated in our previously published work (Bromfield *et al.*, 2017b). Round spermatids were pre-treated with PD146176 for 15 min prior to exposure to 4HNE, and the inhibitor was retained in the solution for the duration of treatment thereafter (1 h) to ensure adequate inhibition of ALOX15 activity. The function of ACSL4 was inhibited in round spermatids by the application of rosiglitazone. Rosiglitazone is a peroxisome proliferator-activated receptor gamma agonist that selectively inhibits ACSL4 over other ACSL isoforms (Kim *et al.*, 2001; Doll *et al.*, 2017). Rosiglitazone was used at a concentration of 10 µM based on previously published findings using this compound in stallion spermatozoa (Swegen *et al.*, 2016). Cells were pre-treated with rosiglitazone for 30 min before exposure to 4HNE for 1 h at 37°C. Round spermatids were then evaluated for cell death (using PI) and lipid peroxidation levels (using BODIPY c11).

Lipid peroxidation assessment with BODIPY c11

Lipid peroxidation levels were measured using the BODIPY c11 probe (10 µM). This probe was pre-incubated with round spermatid samples for 30 min at 37°C prior to the induction of oxidative stress. Cells were then washed free of the probe with pre-warmed DMEM, and oxidative stress was induced using 4HNE. At the completion of the assay, lipid peroxidation levels were measured using fluorescence microscopy. The shift in BODIPY c11 fluorescence emission upon lipid oxidation (590 to 510 nm) was readily detected as a red to green fluorescence shift, as previously described (Walters *et al.*, 2018), and from this the number of cells possessing green fluorescence was quantified for 100 cells per sample and across three biological replicates.

Statistics

Statistical significance was determined using ANOVA, Tukey–Kramer HSD and Student's *t*-tests employing JMP (version 13.0.0, SAS Institute, North Carolina, USA) and Excel software (Version 15.32, Microsoft, Washington, USA). Differences with a value of $P < 0.05$ were considered to be statistically significant. Each experiment was conducted on a minimum of three biological replicates with each replicate comprising germ cells obtained from 2 to 4 age matched Swiss male mice. All data are expressed as mean ± S.E.M. The level of significance is either denoted by asterisks such that $P < 0.05$ (*), $P < 0.01$ (**) and $P < 0.005$ (***) or through connecting letter reports where mean values without a common superscript differ significantly, $P < 0.05$.

Results

Spermatocytes and spermatids experience different cell death modalities after 4HNE exposure

To establish the dependency of spermatocytes and spermatids on caspase-regulated cell death pathways elicited by 4HNE, two correlates of apoptosis were measured across a 4HNE dose response (100–400 µM). As expected from our previous analysis of oxidative stress in developing germ cells (Bromfield *et al.*, 2017b), increasing the dose of 4HNE induced a linear cell death response in both pachytene spermatocytes and round spermatids as measured by propidium iodide (PI) fluorescence (Koppers *et al.*, 2011). Notably, however, a distinct difference in the response of pachytene spermatocytes and round spermatids to 4HNE-exposure was highlighted through our analysis of FLICA and Annexin V fluorescence across the same dose curve

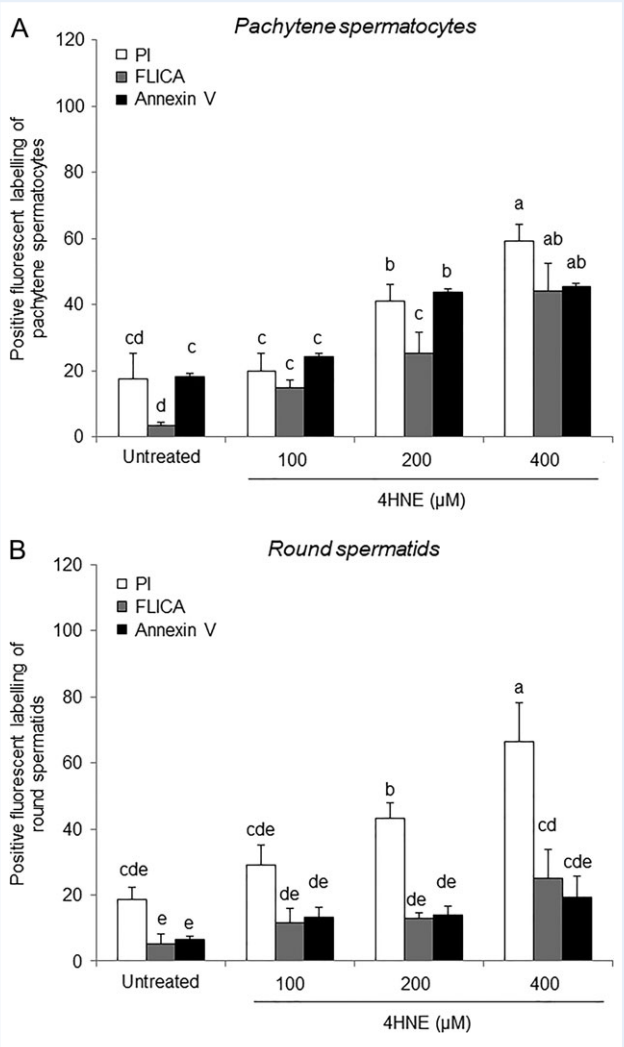

Figure 1 Differences in cell death responses between mouse pachytene spermatocytes and round spermatids following 4-hydroxynonenal exposure. Oxidative stress was induced in pachytene spermatocytes and round spermatids through increasing doses of 4-hydroxynonenal (4HNE) (100–400 μM). Cell death was recorded as an increase in propidium iodide (PI) fluorescence, caspase activation was analysed through use of the probe for the detection of activated caspases and phosphatidylserine externalization was analysed using Annexin V-FITC. (**A** and **B**) Represent the percentage of cells with positive fluorescent labelling after exposure to each probe. Data are plotted as mean ± SEM ($n = 3$). $^{a\text{-}e}$Mean values without a common superscript differ significantly, $P < 0.05$, as determined by ANOVA.

(Fig. 1A). Thus, in pachytene spermatocytes significant increases in the number of FLICA and Annexin V positive cells were noted after exposure to 100 μM 4HNE ($P < 0.05$) and 200 μM 4HNE ($P < 0.01$), respectively (Fig. 1A). Moreover, at the highest dose of 4HNE used (400 μM) there was no significant difference between the number of pachytene spermatocytes positive for PI (dead) and the number of FLICA and Annexin V—positive pachytene spermatocytes, implying synergy between the induction of cell death and the onset of apoptosis as marked by caspase activation (FLICA) and phosphatidylserine externalization (Annexin V). In stark contrast to this, the number of round spermatids positive for FLICA and Annexin V did not account for the significant increase in PI-positive cells induced by increasing doses of 4HNE. Moreover, only the highest dose of 4HNE was able to elicit a small but significant increase in the number of FLICA positive cells compared to the untreated control (Fig. 1B; 25 versus 5%; $P < 0.05$). Consistent with this observation, at both 200 and 400 μM doses of 4HNE there remained a significant difference between the number of PI positive cells (43 and 66%, respectively) and the number of cells expressing markers of apoptosis (FLICA; 13 and 25%, respectively; Annexin V; 14 and 19%).

The divergent response of round spermatids and pachytene spermatocytes to the induction of apoptosis by 4HNE led us to further examine, whether this form of oxidative insult may induce a caspase-independent form of cell death specifically in round spermatids. To investigate this hypothesis in more detail, we employed two recently described ferroptosis activators, erastin and RSL3, which induce ferroptotic cell-death in cancer cells through two independent mechanisms (Shintoku *et al.*, 2017). Notably, exposure of the germ cells to 10–40 μM erastin elicited a rapid and significant decline in the number of viable round spermatids, but no equivalent response was observed in pachytene spermatocytes, implying differential sensitivity of germ cells to the chemical stimulation of ferroptosis (Fig. 2A). The stage-dependent nature of this form of cell death was again demonstrated through the use of 0.1–10 μM RSL3 (Fig. 2B). Indeed, the highest doses of erastin and RSL3 used in this study reduced the viability of round spermatids by 39 and 42%, respectively, within the 1 h exposure period applied. Importantly, this reduction in round spermatid viability was also reflective of the number of non-viable round spermatids recorded after a 1 h exposure to 100 μM 4HNE (29% Fig. 1B). To confirm whether RSL3 and erastin could continue to increase cell death in round spermatids with prolonged time, the cell viability of spermatids was monitored over a 5 h time course following exposure to 100 μM 4HNE, 1 μM RSL3 and 20 μM erastin. Here, all three insults were able to reduce cell viability by >80% by 5 h of incubation (Fig. 2C). Having established parallels between erastin/RSL3-induced cell death and 4HNE-induced cell death in round spermatids, we next sought to evaluate key changes to the round spermatid proteome that could contribute to the onset of ferroptosis in these germ cells. In being cautious not to draw conclusions on protein expression changes in cell populations where >50% of cells were dead, a 1 h incubation time for 4HNE, RSL3 and erastin, where 30–40% cell death could be consistently achieved, was selected for the remaining experiments of this study. This treatment regimen permitted the thorough analysis of cells that were potentially responding to ferroptotic stimuli and undergoing the processes of cell death.

4HNE, erastin and RSL3 induce changes to the proteome consistent with ferroptosis in round spermatids

In this study, three key proteins ALOX15, ACSL4 and GPX4, were targeted for analysis as they are known regulators of ferroptotic cell death in somatic cells (Yang *et al.*, 2014, 2016; Doll *et al.*, 2017). Through immunoblotting with antibodies against ALOX15, ACSL4 and GPX4, distinct changes in the profile of all three proteins were observed. Consistent with our previous studies, 4HNE-induced

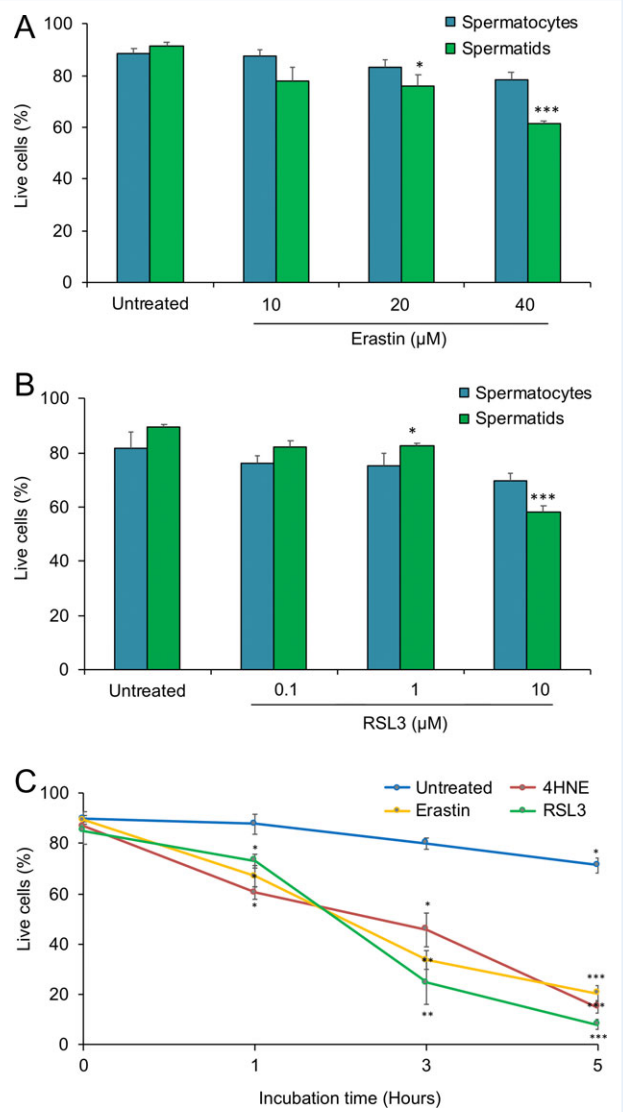

Figure 2 Monitoring the induction of cell death by erastin and RSL3 in male germ cells of the mouse. (**A**) Germ cells were incubated in 10, 20 and 40 μM erastin and (**B**) 0.1, 1 and 10 μM RSL3 to induce ferroptosis. The resulting cell death percentages were determined by recording cells positive for Eosin Y incorporation through the use of light microscopy. (**C**) Using the same method, the percentage of live cells following incubation with 100 μM 4HNE, 20 μM erastin and 1 μM RSL3 over a time course of 5 h was recorded for $t = 0$, $t = 1$, $t = 3$ and $t = 5$ (hours). Data are plotted as mean ± SEM ($n = 5$) and Student's t tests were performed relative to the untreated control. * $P < 0.05$, ** $P < 0.01$, *** $P < 0.001$.

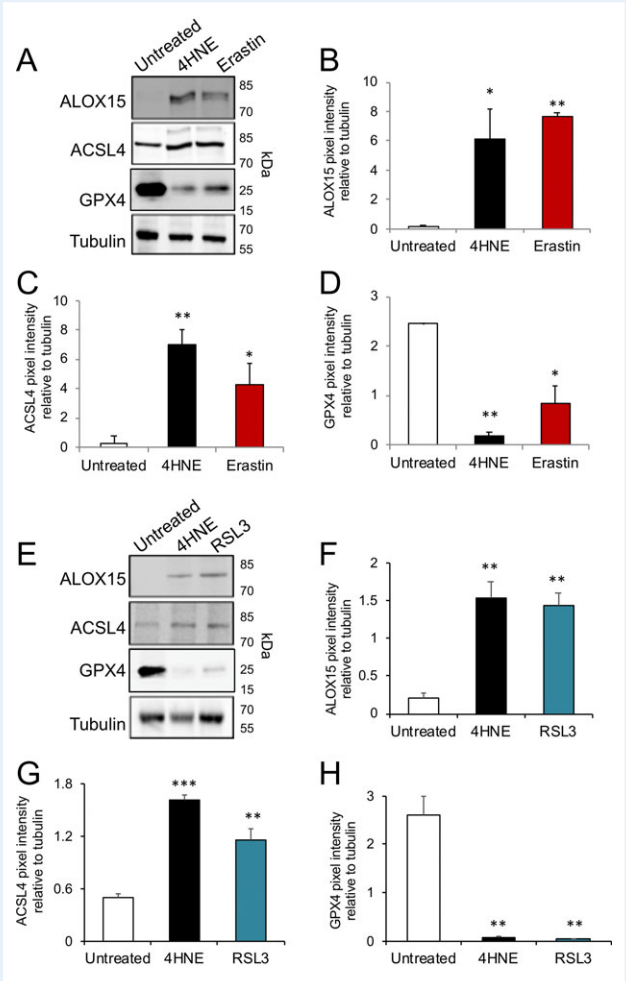

Figure 3 4HNE, erastin and RSL3 induce changes to the mouse germ cell proteome consistent with ferroptosis. Round spermatids were exposed to either 100 μM 4HNE, 20 μM erastin or 1 μM RSL3 for 1 h and then lysed for sodium dodecyl sulphate-polyacrylamide gel electrophoresis and immunoblotting procedures. Immunoblotting was performed using anti-arachidonate 15-lipoxygenase (ALOX15), anti-acyl-CoA synthetase long-chain family member 4 (ACSL4) and anti-glutathione peroxidase 4 (GPX4) antibodies (presented in **A** and **E**) and bands corresponding to proteins of the correct molecular weight were subjected to densitometry analysis relative to their corresponding α-tubulin immunoblot loading controls (**B**–**D** and **F**–**H**). Significant changes in protein expression were determined through Student's *t*-tests relative to the untreated control lane densitometry values ($n = 3$). Note: The amount of protein lysate loaded for each gel was 5 μg for the immunoblots featured in (**A**) and their corresponding replicates and 2.5 μg for immunoblots presented in (**E**) and their corresponding replicates. *$P < 0.05$, **$P < 0.01$, ***$P < 0.001$.

oxidative stress elicited a robust increase in ALOX15 protein levels in round spermatids (Fig. 3A/B and E/F). Moreover, exposure to either erastin (Fig. 3A) or RSL3 (Fig. 3E) also induced a significant increase in ALOX15 protein levels compared to untreated cells ($P < 0.01$); with band density analysis revealing statistical similarity between the responses induced by 4HNE and erastin (Fig. 3B; $P > 0.05$) and 4HNE and RSL3 (Fig. 3F; $P > 0.05$). Additionally, analysis of ACSL4 in round spermatids following 4HNE, erastin and RSL3 treatment revealed a small but significant increase in all three treatment groups compared to the untreated control (Fig. 3G). The statistical relevance of these changes was confirmed through band densitometry analyses of anti-ACSL4 immunoblots relative to tubulin loading controls. Thus, these findings confirm a modest upregulation of ACSL4 during the onset of ferroptosis induced by erastin and

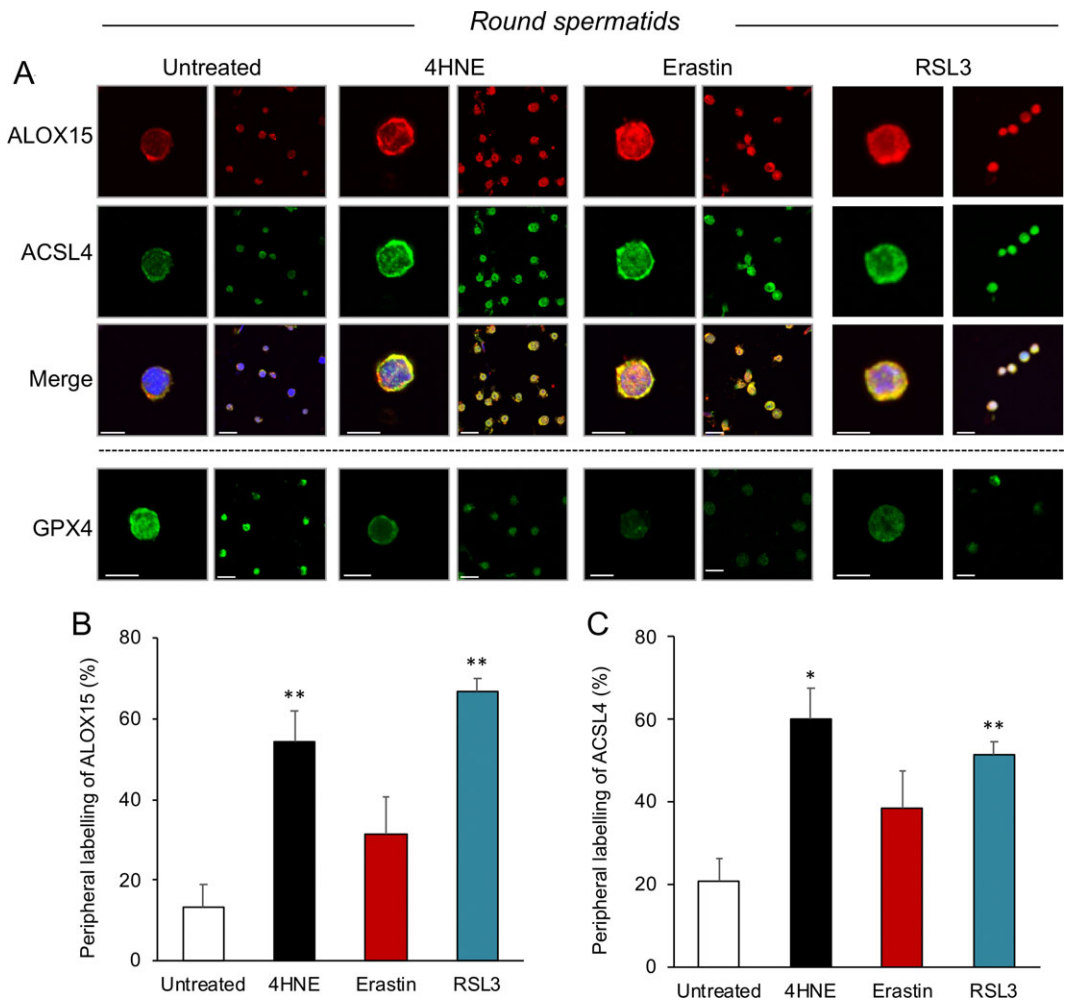

Figure 4 Immunolocalization of ALOX15, ACSL4 and GPX4 in mouse round spermatids in response to ferroptotic stimuli. (**A**) Following the induction of oxidative stress with 4HNE or ferroptosis with erastin and RSL3, immunolocalization was performed in paraformaldehyde fixed round spermatids using antibodies to ALOX15, ACSL4 or GPX4 and corresponding fluorescently labelled secondary antibodies. Co-localization of ALOX15 and ACSL4 was performed by sequential incubation of primary and secondary antibodies and cells were then counterstained with the nuclear stain DAPI. Cell labelling was examined with a Zeiss LSM510 laser scanning confocal microscope. (**B** and **C**) Peripheral membrane localization of ACSL4 and ALOX15 was determined through visualization of round spermatids. The percentage of cells displaying this pattern of ALOX15 and ACSL4 labelling was established by scoring cells as 'positive' when clear peripheral labelling around the circumference of the cell was observed. At least 50 cells per replicate were scored across four biological replicates. Data are presented as mean ± SEM ($n = 4$. *$P < 0.05$; **$P < 0.01$, as verified by Student's t tests). Scale bar = 5 μm.

RSL3 in round spermatids, as well as through 4HNE exposure. The final component of this analysis was the evaluation of GPX4 expression. This is critical, as a decline in GPX4 function is a crucial hallmark of the induction of ferroptosis (Yang *et al.*, 2014). In untreated round spermatids, our anti-GPX4 antibody enabled the detection of GPX4 protein at ~20 kDa, with the antibody epitope sequence best aligned to 'mitochondrial' GPX4. Following 4HNE, erastin and RSL3 exposure, the levels of GPX4 protein labelled through immunoblotting were consistently and significantly reduced (Fig. 3A/E) compared to untreated cell lysates; a result that was confirmed by band densitometry analyses relative to tubulin (Fig. 3D/H). In both cases, the changes in GPX4 protein expression elicited by 4HNE were statistically similar to those induced by both erastin ($P > 0.05$) and RSL3 ($P > 0.05$), highlighting the similarity in cellular response to all three insults.

Following these analyses, visual confirmation of ALOX15, ACSL4 and GPX4 expression in round spermatids was sought through immunocytochemistry of 4HNE, erastin and RSL3-exposed cells. This protocol confirmed the presence of all three proteins in round spermatids with observable differences in the intensity of antibody labelling that were reflective of the trends observed through immunoblotting experiments (Fig. 4A). Moreover, the species compatibility of the ACSL4 and ALOX15 antibodies allowed the co-localization of these proteins to be explored, revealing distinct

co-localization of ACSL4 and ALOX15 in the periphery of the cells (Fig. 4A merge). To confirm whether this peripheral membrane labelling occurred as a function of the treatments applied to round spermatids in culture, the percentage of cells with distinct peripheral labelling of ACSL4 and ALOX15 was recorded (Fig. 4B/C). In performing this analysis, it was revealed that both 4HNE and the GPX4 inhibitor RSL3 were capable of inducing a significant increase in this 'membrane-like' localization of both ALOX15 (Fig. 4B; $P < 0.01$) and ACSL4 (Fig. 4C; $P < 0.01$) compared to the untreated control. Notably, while erastin was able to elicit an increase in ALOX15 and ACSL4 protein expression (Fig. 3), this chemical did not yield a quantifiable difference in the localization of these proteins within round spermatids ($P > 0.05$ compared to untreated). Consistent with our immunoblotting results for GPX4, the expression of this enzyme was markedly reduced in response to 4HNE, erastin and RSL3 treatments (Fig. 4A). With this in mind, the localization of GPX4 was not able to be assessed in response to our experimental conditions due to the loss of protein expression following treatment.

Immunocytochemistry was also performed on pachytene spermatocytes to determine whether 4HNE, erastin or RSL3 elicited changes in the localization of ALOX15, ACSL4 or GPX4. In contrast to round spermatids, exposure of pachytene spermatocytes to these chemicals did not induce overt changes in immunofluorescence compared to the untreated control cells (Fig. 5A). While occasional peripheral membrane labelling was observed in both untreated and treated cell populations, no significant localization change was detected in spermatocytes (Supplementary Fig. S1B–D). Moreover, immunoblotting with antibodies to ALOX15, ACSL4 and GPX4 revealed no change in protein expression in response to 4HNE, erastin or RSL3 (Fig. 5B; Supplementary Fig. S1E).

Having established that oxidative stress resulted in changes to GPX4 that were consistent with ferroptotic cell death, we hypothesized that mature sperm cells may also retain sensitivity to ferroptosis. To examine this prospect, we focused on the use of RSL3 to induce cell death in mature spermatozoa using the same concentration applied to round spermatids (1 μM) in addition to doses that fall 10-fold either side of this (0.1 and 10 μM). To avoid confounding results, erastin was not used to induce cell death in spermatozoa. This decision was based on the rationale that, aside from the induction of ferroptosis, erastin also inhibits the voltage dependent ion channel that supports sperm motility and viability (Sampson *et al.*, 2001; Kwon *et al.*, 2013; Liu *et al.*, 2014). Thus, exposure of spermatozoa to erastin would be expected to induce a loss of cell viability regardless of the propensity of these cells to undergo ferroptosis.

Prior to evaluating the process of ferroptosis in mature spermatozoa, the presence of GPX4 in mouse and human sperm was confirmed through immunoblotting of lysates from untreated, 4HNE-exposed and RSL3-exposed spermatozoa (Fig. 5C/D). In all lysates, GPX4 was detected as a monomer at ~20 kDa. Having established the presence of GPX4 in these cells, we sought to chemically induce ferroptosis through the inhibition of the enzyme with RSL3. Contrary to our hypothesis, the application of RSL3 to inhibit GPX4 in either mouse or human spermatozoa did not result in any significant loss of viability, even at a concentration 10-fold higher than that applied to round spermatids (Fig. 5E/F). These data indicate that the round spermatid stage of mouse sperm development is exclusively susceptible to ferroptotic stimuli such as RSL3.

4HNE-induced cell death in round spermatids can be attenuated by ferrostatin-1 and the iron chelator deferoxamine

The decreased expression of GPX4 and upregulation of ALOX15 and ACSL4 observed in round spermatids exposed to 4HNE was markedly similar to the changes observed upon the induction of ferroptosis by erastin and RSL3. However, to secure a further line of evidence that 4HNE-induced oxidative stress initiates ferroptotic cell death in round spermatids, we used the ferroptosis inhibitor ferrostatin-1 (FER-1) in combination with 4HNE to create an intracellular environment refractory to ferroptosis. Notably, 4HNE-induced cell death was reduced by ~50% ($P < 0.01$) in the presence of FER-1 (Fig. 6A), as demonstrated by the number of cells positive for PI, compared to the 4HNE-alone positive control. This finding confirmed that a substantial portion of the cell death induced by 4HNE was attributable to a ferroptosis-specific pathway. Interestingly though, upon examination of the number of cells exhibiting signals of caspase-dependent cell death, the number of FLICA positive cells was significantly increased following the inhibition of ferroptosis (Fig. 6A; $P < 0.05$). While this increase in apoptotic cells did not completely account for the extent of the reduction in cell death elicited through FER-1, this result may imply some degree of crosstalk between ferroptotic and apoptotic pathways. In confirming the validity of these results, treatment of the round spermatids with FER-1 alone did not modulate the levels of cell death recorded by either PI or FLICA, nor did the DMSO vehicle control (Fig. 6A). As a final correlate of ferroptosis, we examined the dependency of 4HNE-induced cell death on the availability of iron. To evaluate this, the iron chelator deferoxamine (DEF) was used due to its efficacy in preventing ferroptotic cell death in fibrosarcoma cells at a concentration of 100 μM (Dixon *et al.*, 2012). In a similar experimental design to that described for FER-1, DEF was incubated with cells for 1 h prior to the induction of oxidative stress with 4HNE. This strategy led to a significant reduction in oxidative stress induced cell death marked by PI fluorescence (Fig. 6B; $P < 0.05$). However, DEF-mediated chelation of iron did not significantly alter the number of cells positive for FLICA; nor did treatments of DEF alone (Fig. 6B). These results point to the dependency of round spermatids on iron for the induction of ferroptotic cell death.

The inhibition of ALOX15 and ACSL4 prevents lipid peroxidation and cell death in round spermatids

Throughout this study, ALOX15 and ACSL4 were shown to be upregulated in response to oxidative stress in round spermatids. While we have previously explored the inhibition of ALOX15 as a strategy to reduce oxidative stress by using the specific ALOX15 inhibitor PD146176 (Bromfield *et al.*, 2017b), it remained to be determined whether this inhibition strategy could modulate cell death and overall levels of lipid peroxidation in round spermatids. Moreover, ACSL4 is thought to dictate the sensitivity of cells to ferroptosis as it increases the pool of oxidizable lipid (Doll *et al.*, 2017). In this way, ACSL4 also increases the overall rate of ferroptosis. Given this, we were also interested in determining whether the inhibition of ACSL4 could provide a mechanism to suppress ferroptosis in round spermatids. In response to 4HNE exposure, a significant increase in the percentage of round

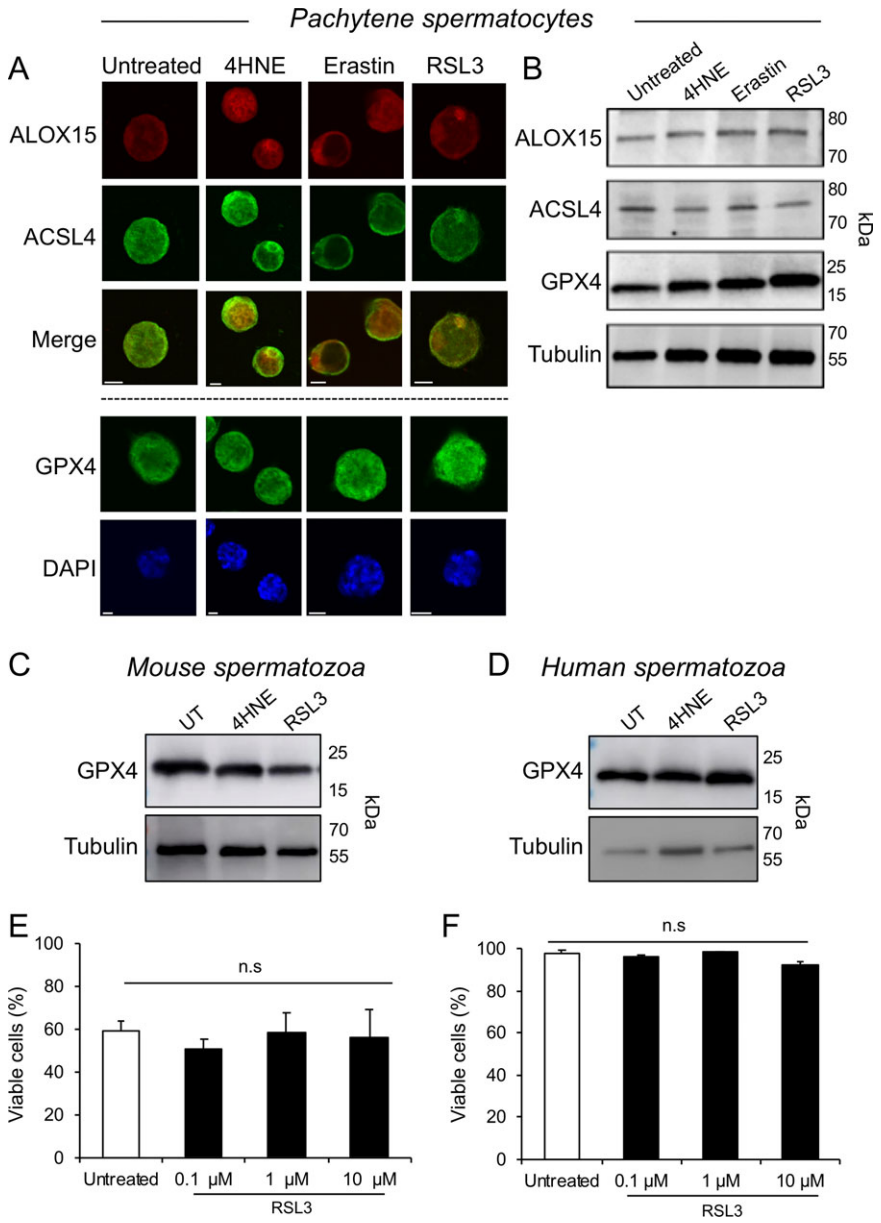

Figure 5 Analysis of mouse pachytene spermatocytes and mouse and human mature spermatozoa following exposure to 4HNE, erastin and RSL3. (**A**) Immunolocalization was performed in paraformaldehyde fixed pachytene spermatocytes using antibodies to ALOX15, ACSL4 or GPX4 and corresponding fluorescently labelled secondary antibodies. Co-localization of ALOX15 and ACSL4 was performed by sequential incubation of primary and secondary antibodies and cells were counterstained with the nuclear marker DAPI. Cell labelling was examined with a Zeiss LSM510 laser scanning confocal microscope. (**B**) Protein lysates were prepared from pachytene spermatocytes exposed to 4HNE, erastin and RSL3 and proteins were separated through SDS-PAGE with 2.5 μg of protein loaded in each lane. Immunoblotting was performed with anti-ALOX15, ACSL4 and GPX4 antibodies and equal protein loading was verified by stripping and reprobing immunoblots with anti-α-tubulin. (**C**, **D**) Immunoblotting with anti-GPX4 antibodies was performed for mouse and human sperm lysates (5 μg per lane) prepared from cells treated with either 4HNE or RSL3 and their corresponding untreated controls. Equal protein loading was verified through immunoblotting with anti-α-tubulin. (**E**, **F**) An RSL3 dose response (0.1–10 μM) was performed in mature mouse and human spermatozoa to assess levels of cell death. Cell death was determined through visualization of Eosin Y incorporation into spermatozoa with data presented as the percentage of viable cells ($n = 3$, mean ± SEM). n.s denotes 'no significance', $P > 0.05$, as determined by Student's t tests. Scale bar = 5 μm.

spermatids exhibiting a positive signal for BODIPY c11 was recorded, indicating a significant increase in membrane lipid peroxidation (Fig. 7A; $P < 0.01$). However, when these treatments were performed in the presence of either 0.5 μM PD146176, to inhibit ALOX15, or 10 μM Rosiglitazone (ROSI), to inhibit ACSL4, significant reductions in BODIPY c11-positive cells were recorded ($P < 0.05$; $P < 0.01$, respectively). Moreover, the use of these inhibitors in tandem (Fig. 7A 'combined') reduced the number of BODIPY c11-positive cells to levels that

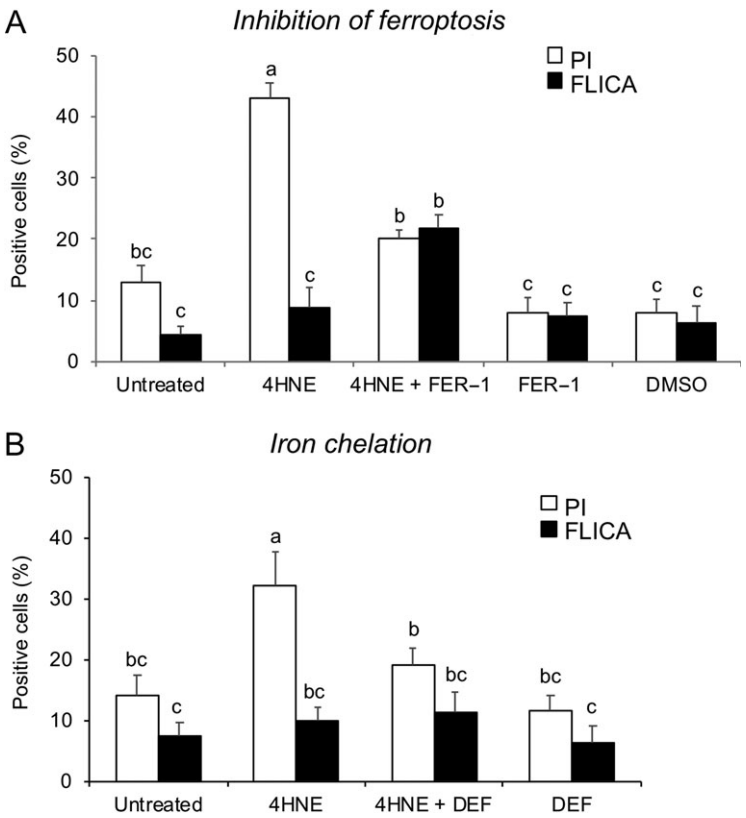

Figure 6 Manipulation of mouse germ cell death with ferrostatin-1 and deferoxamine. (**A** and **B**) The ferroptosis inhibitor; ferrostatin-1 (FER-1; 2 μM), and iron chelator; deferoxamine (DEF; 100 μM), were used in combination with 4HNE to verify the dependency of 4HNE-stimulated cell death in round spermatids on the activation of ferroptotic pathways (**A**) and the availability of labile iron (**B**). Cell death percentages were recorded through the incorporation of propidium iodide (PI) in round spermatids and analysis of cells through fluorescence microscopy. Caspase activation was assessed using the FLICA apoptosis detection kit and positive signals for propidium iodide (PI) and FLICA in round spermatids are expressed as the percentage of positive cells. DEF and FER-1 only controls were included to exclude the influence of these chemicals on cell death, independent of its stimulation by 4HNE. DMSO was included as a vehicle control for FER-1. Data are presented as mean values ± SEM ($n = 3$). Statistical analysis was performed using ANOVA. ^{a,b,c}Mean values without a common superscript differ significantly, $P < 0.05$.

were statistically similar to naive cell populations that had not been exposed to 4HNE ($P > 0.05$; Fig. 7A). Importantly, the incubation of round spermatids in PD146176 and ROSI in the absence of 4HNE yielded no significant changes in levels of lipid peroxidation compared to untreated cells ($P > 0.05$; Fig. 7A). To determine whether the reduction in lipid peroxidation achieved through ALOX15 and ACSL4 inhibition was conducive with the inhibition of ferroptosis and the preservation of cell viability, the number of viable cells was recorded using an Eosin Y exclusion assay (Fig. 7B). As expected, under these conditions of 4HNE exposure, a significant ($P < 0.01$) reduction in cell viability was recorded. While treatments of PD146176 or ROSI alone did not directly influence cell viability, they were both able to significantly attenuate the loss of cell viability when co-administrated alongside 4HNE challenge ($P < 0.05$). This trend was also reflected in combined treatments utilizing both inhibitors ($P < 0.05$; Fig. 7B). These data support the involvement of ALOX15 and ACSL4 in a lipid peroxidation-dependent cell death pathway in round spermatids and highlight the therapeutic potential of interventions that selectively inhibit these enzymes in terms of protecting this vulnerable population of developing germ cells.

Discussion

In recent years there has been a growing appreciation for the role of lipids in the non-apoptotic cell death mechanisms that control the demise of cells. Particularly in the context of sensitizing cancer cells to therapeutics, gaining a precise understanding of how cells die is critical. In this light, several regulated cell death events in mammalian cells are now known to possess signatures of non-apoptotic pathways including necroptosis, pyroptosis, parthantos and autosis (recently reviewed in Parisi *et al.*, 2018; Ye *et al.*, 2018). Further, the characterization of an iron-regulated cellular decline (Dixon *et al.*, 2012) has prompted a rapid reappraisal of cell death modalities in numerous pathological contexts (Müller *et al.*, 2017; Lu *et al.*, 2018). Not only is ferroptosis proving important for the regulation of cancer cell death (Shen *et al.*, 2018) and the pathophysiology of neurodegenerative disorders (Hambright *et al.*, 2017; Morris *et al.*, 2018), the broad significance of this pathway has recently been established through observations of root cells in response to heat shock in the flowering plant *Arabidopsis thaliana* (Distéfano *et al.*, 2017). The similarity of this GPX4-mediated cell decline in animal and plant cells (Conlon and Dixon, 2017) alludes

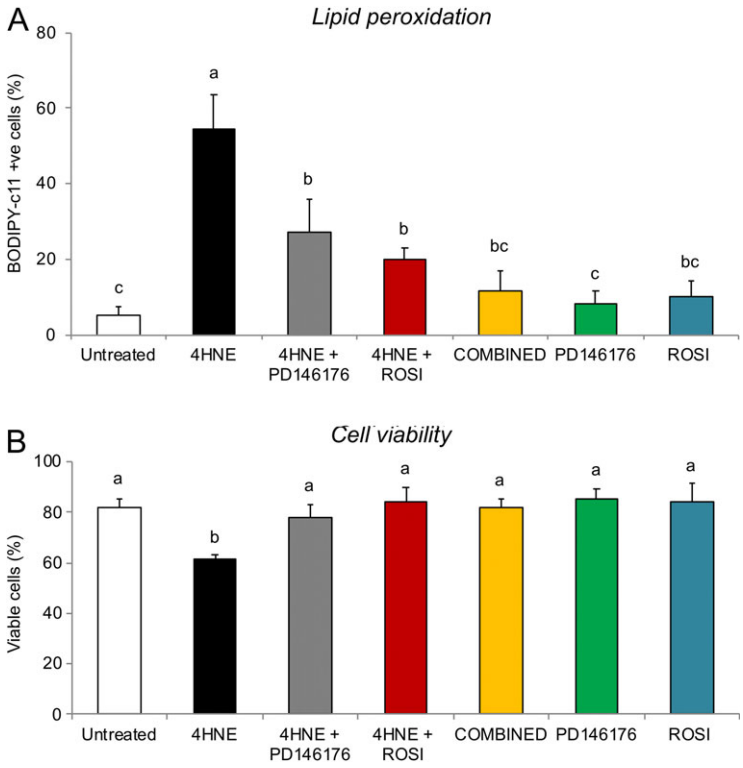

Figure 7 Effect of ALOX15 and ACSL4 inhibition on lipid peroxidation and cell death in round spermatids of the mouse. Inhibition of ALOX15 activity in round spermatids was performed using the indole-based inhibitor PD146176 at a concentration of 0.5 μM. The function of ACSL4 was inhibited through incubation of the cells in 10 μM rosiglitazone. For both inhibitors, cells were pre-treated for 30 min prior to the induction of oxidative stress and ferroptosis with 4HNE and then PD146176 and rosiglitazone (ROSI) were retained for the duration of 4HNE exposure. Controls of PD146176 and ROSI alone were included and the combination of the inhibitors (COMBINED) was trialled. Following incubation, lipid peroxidation was measured in round spermatids (**A**) by recording the percentage of cells positive for green BODIPY c11 fluorescence (emission = 510 nm). Cell viability was recorded using an Eosin Y exclusion assay (**B**) with data presented as the percentage of viable cells. Statistical analysis was performed using ANOVA and post-hoc analysis (Tukey–Kramer's HSD test) and data are presented as mean ± SEM ($n = 3$). ^{a,b,c}Mean values without a common superscript differ significantly, $P < 0.05$.

to the possibility that ferroptosis may be a highly conserved mechanism to respond to acute stress that is evolutionarily ancient, though only recently characterized (Distéfano *et al.*, 2017; Conrad *et al.*, 2018). Building on these discoveries, here we present the first findings of ferroptosis outside of the soma, and provide evidence for the exclusivity of this process to the round spermatid stage of testicular sperm development. Further, this is the first account of ferroptotic induction following exposure to the lipid peroxidation product 4HNE, highlighting the innate cyclicity of lipid-reactive oxygen species (ROS) production in the male germline. Herein, we discuss the unique biochemistry of round spermatids that permits this form of cell death, the utility of targeting ALOX15 and ACSL4 to reduce the sensitivity of cells to lipid peroxidation, and the implications of these findings for fertility regulation.

Cells undergoing ferroptosis do not exhibit morphological or biochemical features typical of apoptosis, such as chromatin margination, plasma membrane blebbing, nuclear fragmentation or cleavage of poly ADP-ribose polymerase (Cao and Dixon, 2016). Rather, ferroptosis is characterized by the shrinkage of organelles, especially mitochondria, a reduction of mitochondria crista, and maintenance of a normal nuclear size. Moreover, this pathway is executed independent of the activation of caspase enzymes and intrinsic apoptotic effectors BAX and BCL-2 antagonist/killer 1 (Xie *et al.*, 2016). Interestingly, ferroptosis tends to be pro-inflammatory while apoptosis is often anti-inflammatory and immune silent (Galluzzi *et al.*, 2012; Xie *et al.*, 2016). Though little is understood regarding crosstalk between these pathways, the induction of ferroptosis may be refractory to apoptosis as the reducing power of GSH is required for the processing and activation of caspases 3 and 8 (Ueda *et al.*, 1998; Hentze *et al.*, 2002). Cells undergoing ferroptosis have been reported to possess only 10% of the normal levels of intracellular GSH, thus these cells may not have the capacity to activate caspases (Skouta *et al.*, 2014; Dixon, 2017). Furthermore, the inhibition of GSH synthesis has been demonstrated to switch the mode of cell death in U-937 cells from apoptosis to necrosis (Troyano *et al.*, 2001; Dixon, 2017). In our study, inhibition of 4HNE-induced ferroptosis with ferrostatin-1, a molecule that prevents the accumulation of ROS from lipid oxidation (Dixon *et al.*, 2012), in turn promoted a degree of caspase activation, as marked by a significant increase in FLICA fluorescence in round spermatids. This suggests that those cells undergoing ferroptosis may have been prohibited from entering caspase-dependent

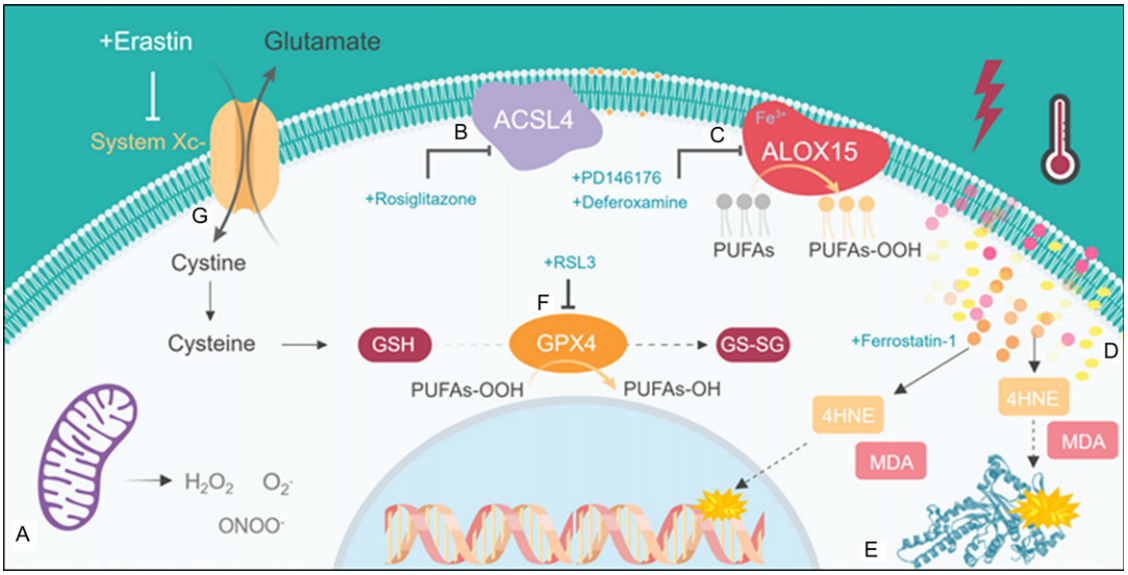

Figure 8 Biochemical elements responsible for the induction of ferroptosis in round spermatids. Exposure to 4HNE results in the modification of mitochondrial proteins such as succinate dehydrogenase and a subsequent elevation of intracellular reactive oxygen species through leakage from the electron transport chain (**A**). These oxidative stress conditions elicit an increased expression of ACSL4 and ALOX15. Increased ACSL4 may result in the incorporation of long-chain fatty acids into the plasma membrane, sensitizing spermatids to ferroptosis (**B**). When iron is available, increased ALOX15 expression catalyzes the oxygenation and degradation of lipids (**C**) to produce lipid hydroperoxides, the death signals of ferroptosis. The breakdown of these lipid reactive oxygen species results in the production of reactive aldehydes (**D**) such as 4HNE and malondialdehyde (MDA), which cause both DNA and protein damage (**E**). In the absence of correct GPX4 function or expression (**F**) these lipid hydroperoxides cannot be metabolized, leading to toxic levels of lipid hydroperoxides and lipid aldehydes and a loss of cell viability (ferroptosis). In this study, ferroptosis was induced either through cysteine deprivation by erastin-mediated inhibition of System Xc^-, which is responsible for the import of cysteine, a key building block for the synthesis of glutathione (**G**), or by directly inhibiting the function of GPX4 with RSL3. Additionally, lipid peroxidation and ferroptotic cell death could be attenuated through the use of rosiglitazone to inhibit ACSL4, PD146176 to inhibit ALOX15 or through the ferroptosis inhibitor ferrostatin-1. Finally, the iron dependency of this cell death pathway was confirmed using the iron chelator, deferoxamine. Taken together, these data point to the activation of ferroptosis in response to 4HNE-induced oxidative stress in round spermatids and identifies several key candidates that could be targeted for therapeutic manipulation to suppress ferroptosis in the germline. GSH, glutathione; GSSG, oxidized glutathione; PUFAs, polyunsaturated fatty acids; PUFAs-OOH, lipid hydroperoxides; H_2O_2, hydrogen peroxide; O_2^-, superoxide anion; $ONOO^-$, peroxynitrite; Fe^{3+}, Ferric iron. Figure created with BioRender.

cell death pathways. These findings open up intriguing lines of enquiry regarding the complexity of cell death regulation in the germline, though the potential for crosstalk between these pathways still requires further validation in both germ line and somatic cells.

Regardless of cell physiology, the onset of ferroptosis correlates with the accumulation of lipid peroxidation markers such as 4HNE and malondialdehyde. Accordingly, cell death occurring exclusively by ferroptosis can be readily suppressed by inhibitors of lipid peroxidation (such as the ALOX15 inhibitor PD146176); iron chelators (such a deferoxamine); lipophilic antioxidants (such as α-tocopherol); as well as through the depletion of PUFAs (Xie *et al.*, 2016; Feng and Stockwell, 2018). In regard to PUFAs, a key difference in the sensitivity of pachytene spermatocytes and round spermatids to this process may lie in the increased incorporation of PUFAs into the round spermatid membrane during development (Oresti *et al.*, 2010). Specifically, in rodent models, round spermatids become enriched in very long-chain fatty acids derived from AA (Oresti *et al.*, 2010). This is a hallmark of germ cell sensitivity to oxidative attack that persists throughout spermiogenesis to produce mature cells that are highly enriched in PUFAs but depleted of key cytoplasmic antioxidants (Aitken *et al.*, 2012). In keeping with these findings, independent studies have demonstrated that ferroptotic cell death is exacerbated in the presence of longer and more unsaturated fatty acids such as AA and its derivatives (Doll *et al.*, 2017). Accordingly, our analysis of the basal levels of lipid aldehydes in pachytene spermatocytes and round spermatids has previously revealed the elevated presence of protein-bound 4HNE in round spermatid cell lysates (Bromfield *et al.*, 2017a). Acknowledging that ALOX15 also undergoes a stage-specific upregulation in response to oxidative stress in round spermatids (Bromfield *et al.*, 2017b), spermatids appear innately more sensitive to ferroptotic cell death than spermatocytes. Indeed, we demonstrate here that round spermatids but not pachytene spermatocytes exhibit hallmarks of ferroptosis that include; a caspase-independent decline in viability following 4HNE exposure, sensitivity to cell death induced by both erastin and RSL3; and changes in the proteome, such as the upregulation of ACSL4 and down-regulation of GPX4 protein expression, which are important features of ferroptosis in somatic cells (Dixon *et al.*, 2012; Yuan *et al.*, 2016). Given these findings, we propose that round spermatids preferentially undergo ferroptosis under conditions of oxidative stress and may be sensitized to this process through the

action of ALOX15 in the generation of lipid hydroperoxides and through the role of ACSL4 in shaping lipid composition in a manner that is conducive to peroxidation (summarized in Fig. 8).

Acyl-CoA synthetases are essential enzymes for the metabolism of lipids. ACSL4 is distinguished from other ACSL isoforms by its marked preference for long-chain PUFAs, such as AA or adrenic acid, where it catalyzes the esterification of CoA to free fatty acids, and activates them for fatty acid oxidation or lipid biosynthesis (Küch *et al.*, 2014). In doing so, ACSL4 greatly increases the pool of oxidizable lipid available in the cell (Doll *et al.*, 2017). Given the increase in ACSL4 expression we observed in round spermatids in response to 4HNE, erastin and RSL3, we expect that this enzyme may be an important regulator of ferroptotic cell death in the germline, as has been demonstrated in elegant studies of human liver carcinoma cells (HEPG2) (Yuan *et al.*, 2016) and mouse embryonic fibroblasts (Doll *et al.*, 2017). In support of this proposal, the inhibition of ACSL4 with rosiglitazone in our study resulted in the protection of round spermatids from 4HNE-induced lipid peroxidation and cell death. Coupled with our findings that ALOX15 inhibition, either in combination with ACSL4 inhibitors or alone, could also significantly suppress cell death as measured by PI incorporation, we propose that these two proteins form key targets to manipulate ferroptosis in round spermatids and should be the subject of further evaluation *in vivo*. While not a focus of the present study, another lipid metabolism gene encoding lysophosphatidylcholine acyltransferase 3 (*Lpcat3*) has been implicated in regulating the sensitivity of cells to ferroptosis. LPCAT3 is one of the enzymes responsible for the insertion of PUFAs into membrane phospholipids and has been found to shape membrane composition in a manner favourable to peroxidation and the initiation of ferroptotic cell death (Dixon *et al.*, 2015). Interestingly, through targeted examination of a highly comprehensive single cell transcriptome data set produced by Hermann *et al.* (2018) it was found that some spermatid subsets display higher *Lpcat3* gene expression, with spikes in expression in cell clusters corresponding to mid and late mouse spermatid development (Hermann BP, personal communication, 15 January 2019). Thus, differences in membrane lipid composition, such as those that arise through the action of LPCAT3, may provide an insight into why only a subset of round spermatids appear to readily enter a ferroptotic cell death cascade when induced by 4HNE or RSL3 in our study. Indeed, LPCAT3 forms an intriguing target as a potential regulator of this process during spermatogenesis.

Notwithstanding our findings that round spermatids undergo ferroptosis in response to stress, a biological rationale for the particular vulnerability of spermatids to this form of cell death remains to be determined. One hypothesis is that this post-meiotic stage of development may form an important quality control checkpoint for cells exiting the testis. In this way, ferroptosis may provide a rapid means of eliminating poor quality cells prior to epididymal transit and as such, may perform an important physiological function in ensuring DNA integrity in the germline. This accords with findings that cells in a state of GSH depletion are more vulnerable to DNA damage (Saez *et al.*, 1993; Chatterjee, 2013). Though this hypothesis requires validation, our findings certainly suggest that the round spermatid developmental programme may be a particularly critical window of cell fate in the testis. Notably, the GPX4 protein only exists as a soluble peroxidase through to the round spermatid stage after which it is found in its catalytically inactive, highly cross-linked form in mature sperm cells where it forms a component of the mitochondrial capsule (Imai *et al.*, 2009). In accordance with this, our findings demonstrate that mature human and mouse spermatozoa, while possessing GPX4, remain refractory to ferroptotic cell death following exposure to either 4HNE or RSL3 and respond to the former with activation of an intrinsic apoptotic cascade (Aitken *et al.*, 2012).

While a physiological role for ferroptosis in development should not be ruled out, the activation of this pathway in round spermatids in response to an elevation of 4HNE suggests that ferroptotic cell death may be induced under pathological conditions in the testis. In this way, the depletion of GSH and subsequent inactivation of GPX4 could form a streamlined cell-signalling paradigm to respond rapidly to acute stress. We have previously demonstrated that the molecular chaperone HSPA2 is modified by 4HNE in round spermatids (but not spermatocytes) and that this modification leads to its prompt degradation (Bromfield *et al.*, 2017a). Thus, the damage incurred to proteins by 4HNE at this stage of development may form a signature of cellular demise that eventuates in the activation of ferroptotic cell clearance mechanisms. While it remains to be explored in the context of ferroptosis, recent discoveries have causally linked oxidative stress and 4HNE-induced protein damage to the spermatogenic dysfunction that is common to varicocele-derived infertility (Shiraishi and Naito, 2006; Gholirad *et al.*, 2017). Illustrative of this, varicocele is frequently associated with intensive iron toxicity, decreases in antioxidant capacity, high levels of thiol oxidation and enhanced 4HNE production; pathologies which manifest as a significant reduction in the number and quality of post-meiotic germ cells (Duarte *et al.*, 2010; Gong *et al.*, 2012; Jensen *et al.*, 2017). Given the clear parallel between these distinctive hallmarks and those conducive to ferroptosis, it is possible that enzymes such as ALOX15 may catalyze varicocele-induced oxidative stress and promote the ferroptotic demise of germ cells at the vulnerable round spermatid stage of development. Interestingly, polymorphisms of glutathione S-transferase (GST), the enzyme that conjugates reduced GSH to its substrates for detoxification, are known to increase susceptibility to infertility in men with varicocele testes, with a significantly higher frequency of the GSTM1 null genotype found amongst varicocele patients (Chen *et al.*, 2002; Zhu *et al.*, 2015). Additionally, GPX-defective spermatozoa were observed in 26% of infertile men diagnosed with oligoasthenozoospermia (Imai *et al.*, 2001), with independent studies also suggesting that the expression of GPX4 may be associated with oligoasthenozoospermia (Diaconu *et al.*, 2006). Given these findings, future studies should be targeted to examining signatures of ferroptosis in infertile men in response to acute periods of oxidative stress in the testis such as those induced by varicocele, torsion or localized heat stress.

In summary, this study has revealed a clear modulation of key elements of the ferroptosis pathway in 4HNE-stressed round spermatids. These discoveries enhance our understanding of the events that underpin germ cell dysfunction and provide a clear impetus to explore the utility of targeting lipid machinery, such as ALOX15 and ACSL4, to reduce the sensitivity of germline cells to lipid peroxidation. Conversely, the unique susceptibility of round spermatids to ferroptosis and the tightly regulated nature of this cell death modality opens up new avenues for the manipulation of this pathway as a novel, and potentially reversible, contraceptive strategy targeted to an depletion of post-meiotic spermatids.

Supplementary data

Supplementary data are available at *Molecular Human Reproduction* online.

Acknowledgements

The authors gratefully acknowledge Jodie Powell for coordinating the human sperm donors used in this study. Additional thanks go to Dr Zamira Gibb and Dr Aleona Swegen for the provision of rosiglitazone for use in this study and for technical assistance. E.G.B. would like to gratefully acknowledge Bob and Terry Kennedy for their generous support.

Authors' roles

E.G.B. conceived of the study, performed the experiments and wrote the article. J.L.H.W. performed key experiments that contributed to the design of the study and greatly assisted with data interpretation, S. L.C., I.R.B., S.J.S. and A.L.A. all provided considerable technical assistance and contributed to experiments in the article, R.J.A contributed to study design and interpretation of findings and edited the article, E. A.M., M.D.D. and B.M.G. contributed to data interpretation and article editing. B.N. contributed to study design, data interpretation, article preparation and editing.

Funding

National Health and Medical Research Council (NHMRC) Early Career Fellowship to E.G.B. (APP1138701), an NHMRC Project Grant (APP1101953) to B.N., R.J.A. and E.A.M., and an NHMRC Project Grant (APP1163319) to B.N., E.G.B. and R.J.A. E.G.B. also received funding support from The University of Newcastle, School of Environmental and Life Sciences and project funding from Bob and Terry Kennedy and the Hunter Medical Research Institute.

Conflict of interest

All authors declare no conflict of interest.

References

Aitken RJ, Harkiss D, Buckingham D. Relationship between iron-catalysed lipid peroxidation potential and human sperm function. *J Reprod Fertil* 1993;**98**:257–265.

Aitken RJ, Whiting S, De Iuliis GN, McClymont S, Mitchell LA, Baker MA. Electrophilic aldehydes generated by sperm metabolism activate mitochondrial reactive oxygen species generation and apoptosis by targeting succinate dehydrogenase. *J Biol Chem* 2012;**287**:33048–33060.

Ayala A, Muñoz MF, Argüelles S. Lipid peroxidation: production, metabolism, and signaling mechanisms of malondialdehyde and 4-hydroxy-2-nonenal. *Oxid Med Cell Longev* 2014;**2014**:1–31.

Baleato RM, Aitken RJ, Roman SD. Vitamin A regulation of BMP4 expression in the male germ line. *Dev Biol* 2005;**286**:78–90.

Björndahl L, Barratt CL, Mortimer D, Jouannet P. How to count sperm properly': checklist for acceptability of studies based on human semen analysis. *Hum Reprod* 2016;**31**:227–232.

Bromfield EG, Aitken RJ, Anderson AL, McLaughlin EA, Nixon B. The impact of oxidative stress on chaperone-mediated human sperm-egg interaction. *Hum Reprod* 2015;**30**:2597–2613.

Bromfield EG, Aitken RJ, McLaughlin EA, Nixon B. Proteolytic degradation of heat shock protein A2 occurs in response to oxidative stress in male germ cells of the mouse. *Mol Hum Reprod* 2017a;**23**:91–105.

Bromfield EG, Mihalas BP, Dun MD, Aitken RJ, McLaughlin EA, Walters JLH, Nixon B. Inhibition of arachidonate 15-lipoxygenase prevents 4-hydroxynonenal-induced protein damage in male gern cells. *Biol Reprod* 2017b;**96**:598–609.

Brütsch SH, Rademacher M, Roth SR, Müller K, Eder S, Viertel D, Franz C, Kuhn H, Borchert A. Male subfertility induced by heterozygous expression of catalytically inactive glutathione peroxidase 4 is rescued in vivo by systemic inactivation of the Alox15 gene. *J Biol Chem* 2016;**291**: 23578–23588.

Cao JY, Dixon SJ. Mechanisms of ferroptosis. *Cell Mol Life Sci* 2016;**73**: 2195–2209.

Chatterjee A. Reduced glutathione: a radioprotector or a modulator of DNA-repair activity? *Nutrients* 2013;**5**:525–542.

Chen SS, Chang LS, Chen HW, Wei YH. Polymorphisms of glutathione S-transferase M1 and male infertility in Taiwanese patients with varicocele. *Hum Reprod* 2002;**17**:718–725.

Chen ZH, Niki E. 4-hydroxynonenal (4-HNE) has been widely accepted as an inducer of oxidative stress. Is this the whole truth about it or can 4-HNE also exert protective effects? *IUBMB Life* 2006;**58**:372–373.

Chen Y, Peng C, Abraham SA, Shan Y, Guo Z, Desouza N, Cheloni G, Li D, Holyoake TL, Li S. Arachidonate 15-lipoxygenase is required for chronic myeloid leukemia stem cell survival. *J Clin Invest* 2014;**124**:3847.

Chu J, Li J, Giannopoulos P, Blass B, Childers W, Abou-Gharbia M, Pratico D. Pharmacologic blockade of 12/15-lipoxygenase ameliorates memory deficits, Aβ and tau neuropathology in the triple-transgenic mice. *Mol Psychiatry* 2015;**20**:1329.

Conlon M, Dixon SJ. Ferroptosis-like death in plant cells. *Mol Cell Oncol* 2017;**4**:e1302906.

Conrad M, Kagan VE, Bayir H, Pagnussat GC, Head B, Traber MG, Stockwell BR. Regulation of lipid peroxidation and ferroptosis in diverse species. *Genes Dev* 2018;**32**:602–619.

Dächert J, Schoeneberger H, Rohde K, Fulda S. RSL3 and erastin differentially regulate redox signaling to promote Smac mimetic-induced cell death. *Oncotarget* 2016;**7**:63779–63792.

Diaconu M, Tangat Y, Böhm D, Kühn H, Michelmann HW, Schreiber G, Haidl G, Glander HJ, Engel W, Nayernia K. Failure of phospholipid hydroperoxide glutathione peroxidase expression in oligoasthenozoospermia and mutations in the PHGPx gene. *Andrologia* 2006;**38**:152–157.

Distéfano AM, Martin MV, Córdoba JP, Bellido AM, D'Ippólito S, Colman SL, Soto D, Roldán JA, Bartoli CG, Zabaleta EJ *et al*. Heat stress induces ferroptosis-like cell death in plants. *J Cell Biol* 2017;**216**:463–476.

Dixon SJ, Lemberg KM, Lamprecht MR, Skouta R, Zaitsev EM, Gleason CE, Patel DN, Bauer AJ, Cantley AM, Yang WS *et al*. Ferroptosis: an iron-dependent form of nonapoptotic cell death. *Cell* 2012;**149**:1060–1072.

Dixon SJ, Patel DN, Welsch M, Skouta R, Lee ED, Hayano M, Thomas AG, Gleason CE, Tatonetti NP, Slusher BS *et al*. Pharmacological inhibition of cystine-glutamate exchange induces endoplasmic reticulum stress and ferroptosis. *eLife* 2014;**3**:e02523.

Dixon SJ, Winter GE, Musavi LS, Lee ED, Snijder B, Rebsamen M, Superti-Furga G, Stockwell BR. Human haploid cell genetics reveals roles for lipid metabolism genes in nonapoptotic cell death. *ACS Chem Biol* 2015;**10**: 1604–1609.

Dixon SJ. Ferroptosis: bug or feature? *Immunol Rev* 2017;**277**:150–157.

Doll S, Proneth B, Tyurina YY, Panzilius E, Kobayashi S, Ingold I, Irmler M, Beckers J, Aichler M, Walch A *et al*. ACSL4 dictates ferroptosis sensitivity by shaping cellular lipid composition. *Nat Chem Biol* 2017;**13**:91–98.

Doll S, Conrad M. Iron and ferroptosis: a still ill-defined liaison. *IUBMB Life* 2017;**69**:423–434.

Duarte F, Blaya R, Telöken PE, Becker D, Fernandes M, Rhoden EL. The effects of N-acetylcysteine on spermatogenesis and degree of testicular

germ cell apoptosis in an experimental model of varicocele in rats. *Int Urol Nephrol* 2010;**42**:603–608.

Feng H, Stockwell BR. Unsolved mysteries: How does lipid peroxidation cause ferroptosis? *PLoS Biol* 2018;**16**:e2006203.

Galluzzi L, Vitale I, Abrams JM, Alnemri ES, Baehrecke EH, Blagosklonny MV, Dawson TM, Dawson VL, El-Deiry WS, Fulda S *et al*. Molecular definitions of cell death subroutines: recommendations of the Nomenclature Committee on Cell Death. *Cell Death Differ* 2012;**19**: 107–120.

Gaschler MM, Stockwell BR. Lipid peroxidation and cell death. *Biochem Biophys Res Commun* 2017;**482**:419–425.

Gassmann M, Grenacher B, Rohde B, Vogel J. Quantifying Western Blots: pitfalls of densitometry. *Electrophoresis* 2009;**30**:1845–1855.

Gholirad S, Razi M, Hassani Bafrani H. Tracing of zinc and iron in experimentally induced varicocele: correlation with oxidative, nitrosative and carbonyl stress. *Andrologia* 2017;**49**:e12687.

Gong S, San Gabriel MC, Zini A, Chan P, O'Flaherty C. Low amounts and high thiol oxidation of peroxiredoxins in spermatozoa from infertile men. *J Androl* 2012;**33**:1342–1351.

Hambright WS, Fonseca RS, Chen L, Na R, Ran Q. Ablation of ferroptosis regulator glutathione peroxidase 4 in forebrain neurons promotes cognitive impairment and neurodegeneration. *Redox Biol* 2017;**12**:8–17.

Hentze H, Schmitz I, Latta M, Krueger A, Krammer PH, Wendel A. Glutathione dependence of caspase-8 activation at the death inducing signaling complex. *J Biol Chem* 2002;**277**:5588–5595.

Hermann BP, Cheng K, Singh A, Roa-De La Cruz L, Mutoji KN, Chen IC, Gildersleeve H, Lehle JD, Mayo M, Westernstroer B *et al*. The mammalian spermatogenesis single-cell transcriptome, from spermatogonial stem cells to spermatids. *Cell Rep* 2018;**25**:1650–1667.

Hu W, Feng Z, Eveleigh J, Iyer G, Pan J, Amin S, Chung FL, Tang MS. The major lipid peroxidation product, trans-4-hydroxy-2-nonenal, preferentially forms DNA adducts at codon 249 of human p53 gene, a unique mutational hotspot in hepatocellular carcinoma. *Carcinogenesis* 2002;**23**: 1781–1789.

Imai H, Suzuki K, Ishizaka K, Ichinose S, Oshima H, Okayasu I, Emoto K, Umeda M, Nakagawa Y. Failure of the expression of phospholipid hydroperoxide glutathione peroxidase in the spermatozoa of human infertile males. *Biol Reprod* 2001;**64**:674–683.

Imai H, Hakkaku N, Iwamoto R, Suzuki J, Suzuki T, Tajima Y, Konishi K, Minami S, Ichinose S, Ishizaka K *et al*. Depletion of selenoprotein GPx4 in spermatocytes causes male infertility in mice. *J Biol Chem* 2009;**284**: 32522–32532.

Ingold I, Aichler M, Yefremova E, Roveri A, Buday K, Doll S, Tasdemir A, Hoffard N, Wurst W, Walch A *et al*. Expression of a catalytically inactive mutant form of glutathione peroxidase 4 (Gpx4) confers a dominant-negative effect in male fertility. *J Biol Chem* 2015;**290**:14668–14678.

Ivanov I, Heydeck D, Hofheinz K, Roffeis J, O'Donnell VB, Kuhn H, Walther M. Molecular enzymology of lipoxygenases. *Arch Biochem Biophys* 2010;**503**:161–174.

Jensen CFS, Østergen P, Dupree JM, Ohl DA, Sønksen J, Fode M. Varicocele and male infertility. *Nat Rev Urol* 2017;**14**:523–533.

Kim JH, Lewin TM, Coleman RA. Expression and characterization of recombinant rat Acyl-coA synthetases 1, 4 and 5. Selective inhibition by triacsin C and thiazolidinediones. *J Biol Chem* 2001;**276**:24667–24673.

Koppers AJ, Mitchell LA, Wang P, Lin M, Aitken RJ. Phosphoinositide 3-kinase signalling pathway involvement in a truncated apoptotic cascade associated with motility loss and oxidative DNA damage in human spermatozoa. *Biochem J* 2011;**436**:687–698.

Küch EM, Vellaramkalayil R, Zhang I, Lehnen D, Brügger B, Sreemmel W, Ehehalt R, Poppelreuther M, Füllekrug J. Differentially localized acyl-CoA synthetase 4 isoenzymes mediate the metabolic channeling of fatty acids towards phosphatidylinositol. *Biochim Biophys Acta* 2014;**1841**:227–239.

Kwon WS, Park YJ, Mohamed el-SA, Pang MG. Voltage-dependent anion channels are a key factor of male fertility. *Fertil Steril* 2013;**99**:354–361.

Liu B, Tang M, Han Z, Li J, Zhang J, Lu P, Song N, Wang Z, Yin C, Zhang W. Co-incubation of human spermatozoa with anti-VDAC antibody reduced sperm motility. *Cell Physiol Biochem* 2014;**33**:142–150.

Lu B, Chen XB, Ying MD, He QJ, Cao J, Yang B. The role of ferroptosis in cancer development and treatment response. *Front Pharamcol* 2018;**8**: 992.

Lundqvist A, Sandstedt M, Sandstedt J, Wickelgren R, Hansson GI, Jeppsson A, Hultén LM. The arachidonate 15-lipoxygenase enzyme product 15-HETE is present in heart tissue from patients with ischemic heart disease and enhances clot formation. *PLoS One* 2016;**11**:e0161629.

Maiorino M, Conrad M, Ursini F. GPx4, lipid peroxidation, and cell death: discoveries, rediscoveries, and open issues. *Antioxid Redox Signal* 2018; **29**:61–74.

Mao F, Wang M, Xu WR. The role of 15-LOX-1 in colitis and colitis-associated colorectal cancer. *Inflamm Res* 2015;**64**:661–669.

Martínez-Clemente M, Ferré N, Titos E, Horrillo R, González-Périz A, Morán-Salvador E, López-Vicario C, Miquel R, Arroyo V, Funk CD *et al*. Disruption of the 12/15-lipoxygenase gene (Alox15) protects hyperlipidemic mice from nonalcoholic fatty liver disease. *Hepatology* 2010;**52**: 1980–1991.

Matsushita M, Freigang S, Schneider C, Conrad M, Bornkamm GW, Kopf M. T cell lipid peroxidation induces ferroptosis and prevent immunity to infection. *J Exp Med* 2015;**212**:555–568.

Morris G, Walker AJ, Berk M, Maes M, Puri BK. Cell death pathways: a novel therapeutic approach for neuroscientists. *Mol Neurobiol* 2018;**55**: 5767–5786.

Müller T, Dewitz C, Schmitz J, Schröder AS, Bräsen JH, Stockwell BR, Murphy JM, Kunzendorf U, Krautwald S. Necroptosis and ferroptosis are alternative cell death pathways that operate in acute kidney failure. *Cell Mol Life Sci* 2017;**74**:3631–3645.

Nixon BJ, Katen AL, Stanger SJ, Schjenken JE, Nixon B, Roman SD. Mouse spermatocytes express CYP2E1 and respond to acrylamide exposure. *PLoS One* 2014;**9**:e94904.

Noguchi N, Yamashita H, Hamahara A, Nakamura J, Kühn H, Niki E. The specificity of lipoxygenase-catalyzed lipid peroxidation and the effects of radical-scavenging antioxidants. *Biol Chem* 2002;**383**:619–626.

Oresti GM, Reyes JG, Luquez JM, Osses N, Furland NE, Aveldaño MI. Differentiation-related changes in lipid classes with long-chain and very long-chain polyenoic fatty acids in rat spermatogenic cells. *J Lipid Res* 2010;**51**:2909–2921.

Parisi LR, Morrow LM, Visser MB, Atilla-Gokcumen GE. Turning the spotlight on lipids in non-apoptotic cell death. *ACS Chem Biol* 2018;**13**:506–515.

Probst L, Dächert J, Schenk B, Fulda S. Lipoxygenase inhibitors protect acute lymphoblastic leukemia cells from ferroptotic cell death. *Biochem Pharmacol* 2017;**140**:41–52.

Redgrove KA, Nixon B, Baker MA, Hetherington L, Baker H, Liu DY, Aitken RJ. The molecular chaperone HSPA2 plays a key role in regulating the expression of sperm surface receptors that mediate sperm-egg recognition. *PLoS One* 2012;**7**:e50851.

Sadeghian H, Jabbari A. 15-lipoxygense inhibitors: a patent review. *Exp Opin Ther Pat* 2015;**26**:65–88.

Saez GT, Valls V, Perez-Broseta C, Iradi A, Oliva MR, Bannister JV, Bannister WH. The role of glutathione in protection against DNA damage induced by rifamycin SV And copper(II) Ions. *Free Radic Res Commun* 1993;**19**:81–92.

Sampson MJ, Decker WK, Beaudet AL, Ruitenbeek W, Armstrong D, Hicks MJ, Craigen WJ. Immotile sperm and infertility in mice lacking mitochondrial voltage-dependent anion channel type 3. *J Biol Chem* 2001;**276**:39206–39212.

Sendobry SM, Cornicelli JA, Welch K, Bocan T, Tait B, Trivedi BK, Colbry N, Dyer RD, Feinmark SJ, Daugherty A. Attenuation of diet-induced atherosclerosis in rabbits with a highly selective 15-lipoxygenase inhibitor lacking significant antioxidant properties. *Br J Pharmacol* 1997;**120**:1199–1206.

Shen Z, Song J, Yung BC, Zhou Z, Wu A, Chen X. Emerging strategies of cancer therapy based on ferroptosis. *Adv Mater* 2018;**30**:e1704007.

Shintoku R, Takigawa Y, Yamada K, Kubota C, Yoshimoto Y, Takeuchi T, Koshiishi I, Torii S. Lipoxygenase-mediated generation of lipid peroxides enhances ferroptosis induced by erastin and RSL3. *Cancer Sci* 2017;**108**:2187–2194.

Shiraishi K, Naito K. Generation of 4-hydroxy-2-nonenal modified proteins in testes predicts improvement in spermatogenesis after varicocelectomy. *Fertil Steril* 2006;**86**:233–235.

Skouta R, Dixon SJ, Wang J, Dunn DE, Orman M, Shimada K, Rosenberg PA, Lo DC, Weinberg JM, Linkermann A *et al*. Ferrostatins inhibit oxidative lipid damage and cell death in diverse disease models. *J Am Chem Soc* 2014;**136**:4551–4556.

Smith T, De Iuliis GN, Lord T, Aitken RJ. The senescence-accelerated mouse prone 8 (SAMP8) as a model for oxidative stress and impaired DNA repair in the male germ line. *Reproduction* 2013;**146**:253–262.

Suzuki H, Kayama Y, Sakamoto M, Iuchi H, Shimizu I, Yoshino T, Katoh D, Nagoshi T, Tojo K, Minamino T *et al*. Arachidonate 12/15-lipoxygenase–induced inflammation and oxidative stress are involved in the development of diabetic cardiomyopathy. *Diabetes* 2015;**64**:618–630.

Swegen A, Lambourne SR, Aitken RJ, Gibb Z. Rosiglitizone improves stallion sperm motility, ATP content, and mitochondrial function. *Biol Reprod* 2016;**95**:1–12.

Troyano A, Fernandez C, Sancho P, Blas E, Aller P. Effect of glutathione depletion on antitumor drug toxicity (apoptosis and necrosis) in U-937 human promonocytic cells. The role of intracellular oxidation. *J Biol Chem* 2001;**276**:47107–47115.

Uchida K. 4-Hydroxy-2-nonenal: a product and mediator of oxidative stress. *Prog Lipid Res* 2003;**42**:318–343.

Ueda S, Nakamura H, Masutani H, Sasada T, Yonehara S, Takabayashi A, Yamaoka Y, Yodori J. Redox regulation of caspase 3 (-like) protease activity: regulatory roles of thioredoxin and cytochrome c. *J Immunol* 1998;**161**:6689–6695.

Walters JLH, De Iuliis GN, Dun MD, Aitken RJ, MLaughlin EA, Nixon B, Bromfield EG. Pharmacological inhibition of arachidonate 15-lipoxygenase protects human spermatozoa against oxidative stress. *Biol Reprod* 2018;**98**:784–794.

Wenzel SE, Tyurina YY, Zhao J, St Croix CM, Dar HH, Mao G, Tyurin VA, Anthonymuthu TS, Kapralov AA, Amoscato AA *et al*. PEBP1 wardens ferroptosis by enabling lipoxygenase generation of lipid death signals. *Cell* 2017;**171**:628–641.

Xie Y, Hou W, Song X, Yu Y, Huang J, Sun X, Kang R, Tand D. Ferroptosis: process and function. *Cell Death Differ* 2016;**23**:369–379.

Yamamoto S. 'enzymatic' lipid peroxidation: reactions of mammalian lipoxygenases. *Free Radic Biol Med* 1991;**10**:149–159.

Yang WS, SriRamaratnam R, Welsch ME, Shimada K, Skouta R, Viswanathan VS, Cheah JH, Clemons PA, Shamji AF, Clish CB *et al*. Regulation of ferroptotic cancer cell death by GPX4. *Cell* 2014;**156**:317–331.

Yang WS, Kim KJ, Gaschler MM, Patel M, Shchepinov MS, Stockwell BR. Peroxidation of polyunsaturated fatty acids by lipoxygenses drives ferroptosis. *Proc Natl Acad Sci USA* 2016;**113**:e4966–e4975.

Ye J, Zhang R, Wu F, Zhai L, Wang K, Xiao M, Xie T, Sui X. Non-apoptotic cell death in malignant tumor cells and natural compounds. *Cancer Lett* 2018;**420**:210–227.

Yuan H, Li X, Zhang X, Kang R, Tang D. Identification of ACSL4 as a biomarker and contributor of ferroptosis. *Biochem Biophys Res Commun* 2016;**478**:1338–1343.

Zhong H, Yin H. Role of lipid peroxidation derived 4-hydroxynonenal (4-HNE) in cancer: focusing on mitochondria. *Redox Biol* 2014;**4**:193–199.

Zhu B, Yin L, Zhang JY. Glutathione S-transferase polymorphisms in varicocele patients: a meta-analysis. *Genet Mol Res* 2015;**14**:18851–18858.

Zilka O, Shah R, Li B, Friedmann Angeli JP, Griesser M, Conrad M, Pratt DA. On the mechanism of cytoprotection by ferrostatin-1 and liproxstatin-1 and the role of lipid peroxidation in ferroptotic cell death. *ACS Cent Sci* 2017;**3**:232–243.